BIOCHEMISTRY
including biophysical chemistry & molecular biology

Current Topic

pubs.acs.org/biochemistry

Insights into Protein Structure and Dynamics by Ultraviolet and Visible Resonance Raman Spectroscopy

Ignacio López-Peña, Brian S. Leigh, Diana E. Schlamadinger, and Judy E. Kim*

Department of Chemistry and Biochemistry, University of California at San Diego, 9500 Gilman Drive, La Jolla, California 92093, United States

ABSTRACT: Raman spectroscopy is a form of vibrational spectroscopy based on inelastic scattering of light. In resonance Raman spectroscopy, the wavelength of the incident light falls within an absorption band of a chromophore, and this overlap of excitation and absorption energy greatly enhances the Raman scattering efficiency of the absorbing species. The ability to probe vibrational spectra of select chromophores within a complex mixture of molecules makes resonance Raman spectroscopy an excellent tool for studies of biomolecules. In this Current Topic, we discuss the type of molecular insights obtained from steady-state and time-resolved resonance Raman studies of a prototypical photoactive protein, rhodopsin. We also review recent efforts in ultraviolet resonance Raman investigations of soluble and membrane-associated biomolecules, including integral membrane proteins and antimicrobial peptides. These examples illustrate that resonance Raman is a sensitive, selective, and practical method for studying the structures of biological molecules, and the molecular bonding, geometry, and environments of protein cofactors, the backbone, and side chains.

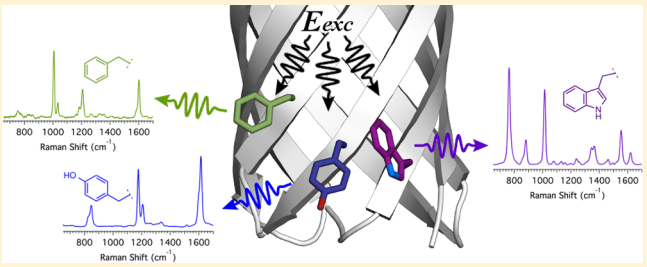

1. INTRODUCTION

The Raman effect was first reported by C. V. Raman in 1928[1,2] and describes inelastic scattering of light from molecules. The difference in energy between the incident and scattered photon corresponds to the vibrational frequency of one of the Raman-active normal modes of the molecule. Hence, Raman spectroscopy reveals vibrational structures. Raman scattering is observed for normal modes that are characterized by a change in polarizability during vibration; in contrast, infrared absorption is associated with a change in dipole moment during vibration. The Raman effect is inherently weak; ~1 in 10^{10} of the incident photons is inelastically scattered in the form of Raman scattering relative to absorption in the form of an infrared transition.[3] The energy of the Raman scattered photon may be lower or higher than that of the incident light. In Stokes Raman scattering, the energy of the scattered photon is lower than that of the incident photon (see Figure 1). When the energy of the scattered photon is higher than that of the incident radiation, the process is called anti-Stokes Raman scattering. Anti-Stokes scattering requires population of higher-lying vibrational states and, therefore, is observed for only low-frequency or hot vibrational modes.

In resonance Raman spectroscopy, the incident wavelength is resonant with an electronic transition. Figure 1 shows both the Stokes and anti-Stokes resonance Raman scattering process. The efficiency of Raman scattering is increased drastically, typically by ~10^3 to 10^6, under resonance conditions.[3−5] Vibrational modes that are coupled to the allowed electronic transition of the absorbing chromophore are selectively enhanced. Fully symmetric modes generally exhibit the strongest enhancements because they can have large displacement (Δ) between ground and resonant excited states (Figure 1).[6] In one limit, the Raman cross section of a mode is proportional to Δ^2. Separate from resonance enhancement, the excitation (E_{exc}) and scattering (E_{scatt}) photon energies also play important roles in determining Raman intensities because the resonance Raman cross section is proportional to $E_{exc}E_{scatt}^3$. This wavelength dependence offers an important advantage for ultraviolet (UV) resonance Raman spectroscopy.

The first biological application of resonance Raman spectroscopy (on carotenoids) appeared in 1932, which is only four years after C.V. Raman first reported the Raman effect.[5] About four decades later, in 1970, Rimai and co-workers published the spectra of carotenoid pigments from carrot root and tomato tissue and of the protein rhodopsin from frozen bovine retinae.[7,8] Raman measurements of the heme structure in hemoglobin[9,10] and cytochrome c[11] were reported afterward. In light of these studies, a strategy for the calculation of resonance Raman scattering was presented by Warshel to facilitate vibrational-mode assignment and the interpretation of spectra from proteins.[12] Today, more than 40 years after the first visible resonance Raman spectrum of a biological system was published, Raman instrumentation is commercially widespread, and visible resonance Raman spectroscopy has become a straightforward tool in biophysics research.

In the case of biological molecules, when the excitation wavelength is tuned to coincide with a UV or visible absorption band of a chromophore, the scattering intensities of the normal

Received: May 11, 2015
Revised: June 28, 2015
Published: July 29, 2015

DOI: 10.1021/acs.biochem.5b00514
Biochemistry 2015, 54, 4770−4783

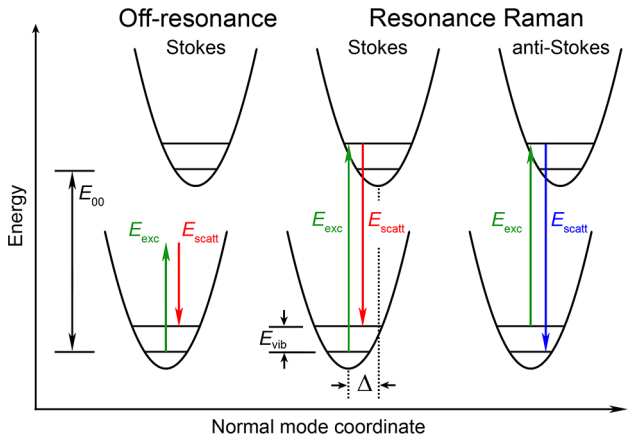

Figure 1. Schematic of the Raman process for a single, harmonic normal mode. Energies of the incident excitation and Raman scattered photons are denoted E_{exc} (green) and E_{scatt} (red and blue), respectively. The zero−zero energy of absorption is denoted E_{00}. Left: off-resonance Raman spectroscopy (Stokes) in which E_{exc} does not coincide with an absorption band. Middle: resonance Raman scattering in which E_{scatt} is lower than E_{exc} (Stokes). Right: resonance Raman spectroscopy in which E_{scatt} is greater than E_{exc} (anti-Stokes). The difference in energy between E_{exc} and E_{scatt} is the Raman shift, denoted E_{vib}, and reflects the vibrational energy of the normal mode. The difference in equilibrium geometry between ground and excited states is denoted Δ.

modes associated with that chromophore are enhanced while Raman intensities of all other normal modes of the biomolecule and aqueous buffer remain weak. In this manner, resonance Raman spectroscopy provides chromophore-specific signal without the need for isotopic labeling or other chemical modification. This specificity contrasts with infrared absorption in which strong signal from IR-active water as well as other molecules is a common problem. This increased sensitivity of resonance Raman allows for the investigation of samples with low concentrations; resonance Raman spectra of micro- to nanomolar concentrations are obtained in minutes. Raman spectroscopy, like other vibrational techniques, has high time and structure sensitivity and can be used to characterize nuclear motions that occur on the timescale of 10^{-13} s and measure changes in bond lengths of ∼0.2 Å.[13] Collectively, these advantages make resonance Raman a valuable method for studying the structures of biological molecules, and the molecular bonding, geometry, and environment of protein cofactors, the backbone, and side chains.

The fact that resonance Raman is capable of yielding structural information with fast time resolution and high selectivity makes it an excellent tool for the study of protein dynamics. Steady-state and time-resolved optical techniques, including resonance Raman spectroscopy, complement high-resolution structural methods in the characterization of electronic and nuclear structures of biological molecules and reaction intermediates. High-resolution methods reveal the average atomic coordinates of the protein ensemble, typically under equilibrium conditions. In addition to static structures, knowledge of the dynamics associated with proteins is essential for fully understanding their varied functions. A broad range of dynamical events over several orders of magnitude in time scale have been probed, such as bond formation and breakage, side-chain rotations, ligand binding, protein folding, and aggregation. The large variation in biologically relevant time scales can be accessed with a variety of methods. X-ray diffraction[14] and multidimensional nuclear magnetic resonance (NMR)[15] techniques remain two of the most powerful structural tools for biomolecules. Optical tools are also essential in the study of proteins. It is now standard to determine reaction kinetics of aqueous protein solutions using continuous-wave (CW) or pulsed lasers combined with rapid-mixing, rapid-flowing, or pump−probe methods. Techniques such as absorption, fluorescence, circular dichroism, and vibrational spectroscopies offer advantages such as minimal sample preparation, dilute solutions, and facile sample recovery. The advent of pulsed lasers has allowed for the measurement of reaction kinetics with femtosecond time resolution, which is comparable to the time scale for molecular vibrations.

We present in this Current Topic biological applications of resonance Raman spectroscopy, with focus on time-resolved studies of a prototypical photoactive protein and recent UV resonance spectroscopy of biomolecules. The first section provides background on the experimental methods, and the second section discusses visible resonance Raman studies of rhodopsin; we have chosen rhodopsin as a prototypical protein to illustrate the depth and breadth of information gained from resonance Raman studies, in particular time-resolved experiments. In the final section, we discuss investigations of the side chains and backbone of soluble and membrane proteins using UV resonance Raman spectroscopy.

2. EXPERIMENTAL METHODS

2.1. Picosecond and Femtosecond Resonance Raman Spectroscopy. The history of visible ultrafast resonance Raman spectroscopy is extensive, and there has been rapid growth in the capabilities of this technique. The first picosecond resonance Raman experiments were conducted in the early 1980s, which is approximately a decade after the first CW experiment was described. In these initial studies of hemoglobin and rhodopsin dynamics, a single-pulse method was used in which pump and probe photons were contained within a single 30 ps pulse.[16,17] Subsequent two-color, pump−probe experiments based on dye lasers and solid-state, Ti:sapphire systems were reported.[18−23] In the dye lasers, tunability was achieved by combinations of dyes and nonlinear frequency conversion methods, such as second-harmonic generation or continuum generation. Ultrafast resonance Raman experiments based on Ti:sapphire systems relied on harmonic generation as well as Raman shifting. The stability and commercial availability of Ti:sapphire lasers further expanded the capabilities of resonance Raman to the femtosecond time regime in femtosecond stimulated Raman spectroscopy (FSRS).[24−27] Given the robust nature and ease of operation of Ti:sapphire systems, ultrafast Raman studies have become common, and numerous reviews of picosecond spontaneous[21−23] and femtosecond stimulated[24−27] resonance Raman experiments have been published. FSRS has become a particularly valuable technique that has allowed investigations of excited-state structures and dynamics. Experimental details will not be described here.

2.2. Ultraviolet Resonance Raman Spectroscopy. UV resonance Raman spectroscopy (UVRR) also has an extensive history of nearly four decades and became widespread as laser and detection systems became more sophisticated. The first UVRR spectra of nucleic acids and UV preresonance Raman spectra of small molecules were acquired in 1975 by a doubled Ar ion laser at 257 nm,[28,29] followed by preresonance Raman

DOI: 10.1021/acs.biochem.5b00514
Biochemistry 2015, 54, 4770−4783

studies of benzene derivatives with a nitrogen dye laser.[30] These and other intracavity-doubled CW lasers are excellent for UVRR experiments because they offer inherently narrow spectral bandwidths that give rise to high-resolution spectra. Additionally, photolysis with CW lasers results in minimal photodamage relative to pulsed systems. The drawback of CW lasers is that they are not tunable, with wavelengths limited to harmonics of the lasing medium; useful wavelengths for UVRR studies of proteins are 228.9 and 206.5 nm from doubled argon and krypton ion lasers, respectively. Greater tunability is achieved with pulsed lasers, including Nd:YAG and Ti:sapphire systems, that pump other media, such as Raman shifters that contain a variety of gases (H_2, D_2, etc.), nonlinear crystals for frequency conversion, and dye lasers.

Currently, the most widespread UVRR systems utilize kilohertz nanosecond Ti:sapphire lasers combined with harmonic generation. In this setup, the laser can typically be tuned from ~700 to 960 nm and the third and fourth harmonics provide wavelengths in the UV region of approximately 195−240 nm.[22,31−35] The advantages of this system are numerous: the high repetition rate minimizes the probability for nonlinear phenomena in the sample, the data collection time is reasonable, nanosecond pulses ensure narrow bandwidths that are suitable for UVRR, and the system is entirely solid-state and, therefore, is robust and straightforward to operate. However, as with all pulsed lasers, high pulse energies can cause significant photodamage, and the concentration of photodamaged sample can continuously increase in the sample reservoir if one utilizes a recirculating system. The 1 kHz repetition rate of a standard Ti:sapphire laser system combined with a single-pass microcapillary flow system is ideal for preventing the accumulation of photoproducts; the illuminated sample volume in a capillary or liquid jet can be replenished between laser pulses, and the photolyzed sample can be discarded. With the right balance among the sample flow rate, capillary diameter, and laser spot size, sample usage and signal can be optimized. For example, a 10 min single-pass Raman measurement of a small (30 kDa) protein may require ≤1 mg of sample for a reasonable signal-to-noise ratio (S/N).

One of the most difficult aspects of UVRR is rejection of Rayleigh scattering. With 228.0 nm excitation, a 200 cm^{-1} Raman-shifted photon has a wavelength of 229.0 nm, which is only 1.0 nm shifted from the excitation wavelength. As a comparison, the same 200 cm^{-1} Raman-shifted photon with 514.5 nm excitation is separated from the excitation wavelength by 5.3 nm. This difference illustrates one of the biggest challenges of UVRR: it is difficult to obtain a commercial UV cutoff filter that can effectively separate 228.0 and 229.0 nm, whereas visible cutoff filters can easily separate 514.5 and 519.8 nm. For this reason, the majority of Rayleigh rejection is accomplished with high-throughput prefilters or other modified dispersing systems. Some examples of filters used in UVRR experiments include low-dispersion, prism-based prefilters,[36−38] modified double monochromators,[32,33,39] and a spatial filter.[40]

3. APPLICATION OF TIME-RESOLVED, VISIBLE RESONANCE RAMAN SPECTROSCOPY

3.1. Protein Chromophores Investigated by Resonance Raman. Visible resonance Raman spectroscopy has been applied to a wide range of colored proteins and related model compounds. Because the Raman effect is weak, chromophores that exhibit low fluorescence and high absorptivity have been the main subjects of this technique. Heme and retinal proteins are ideal for resonance Raman spectroscopy, and as such, these cofactors have been and continue to be studied extensively. Metal−ligand bonds, such as those in iron-containing (e.g., ferredoxin) and copper-containing (e.g., azurin) proteins, have also been investigated by resonance Raman spectroscopy. It has been possible to study fluorescent chromophores, including flavins[41] and chlorophylls,[42,43] using fluorescence rejection techniques, such as gated detection[44,45] and shifted excitation Raman difference spectroscopy (SERDS),[46] as well as fluorescence quenching methods.[41] In the past decade, stimulated Raman spectroscopy has allowed Raman investigations of molecules with near unity fluorescence quantum yields, e.g., laser dyes and fluorescent proteins.[42,47] FSRS has become a powerful modern tool; the combination of femtosecond time resolution and insensitivity to fluorescence has allowed researchers to investigate complex dynamics without complications from fluorescence, such as excited-state proton transfer in green fluorescent protein.[47] Examples of proteins and cofactors investigated via visible resonance Raman spectroscopy are shown in Figure 2. Here we discuss both historical and modern experiments of one of the most widely studied photoactive proteins, rhodopsin.

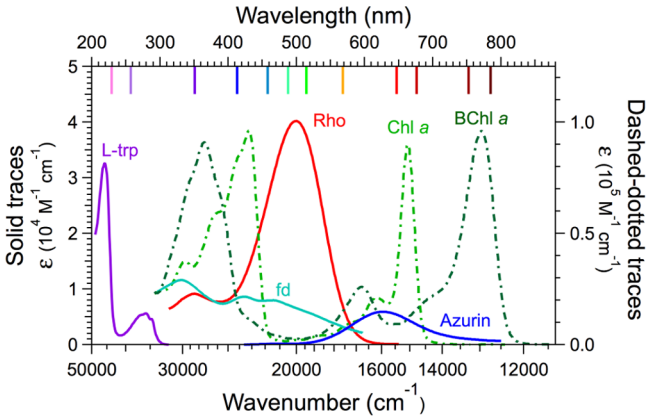

Figure 2. Absorption spectra of some biomolecules studied by resonance Raman spectroscopy. Spectra are for the amino acid L-tryptophan (L-trp), and proteins ferredoxin (fd), bovine rhodopsin (Rho), azurin, chlorophyll *a* (Chl *a*), and bacterial chlorophyll *a* (BChl *a*). Representative excitation wavelengths from frequency-doubled or fundamental lines of argon ion 228.9, 257.2, 351.1, 457.9, 488.0, and 514.5 nm), krypton ion (413.1, 568.2, 647.1, 676.4, and 752.5 nm), and diode (785 nm) lasers are indicated as vertical lines along the top. Note the two scales of molar absorptivity for solid (left axis) and dashed−dotted (right axis) traces. The absorption spectrum of fd is from ref 167, and spectra of Chl *a* and BChl *a* are from refs 168 and 169.

3.2. Rhodopsin. Rhodopsins make up a class of photoreceptors that utilize a retinal chromophore as the light absorber. These proteins are found in eukaryotes, bacteria, and archaea and are essential for organism survival and adaptation to the environment.[48] The two most widely studied retinal proteins are the mammalian visual pigment, rhodopsin, and the microbial proton pump, bacteriorhodopsin. Despite a divergence in function, they share a common mechanism for photoactivation, which is photoisomerization of a retinal chromophore. In both proteins, the retinal chromophores are attached to lysine residues via a protonated Schiff base linkage and are located in the center of a membrane-embedded, seven-α-helix structure. Because of the low fluorescence quantum

DOI: 10.1021/acs.biochem.5b00514
Biochemistry 2015, 54, 4770−4783

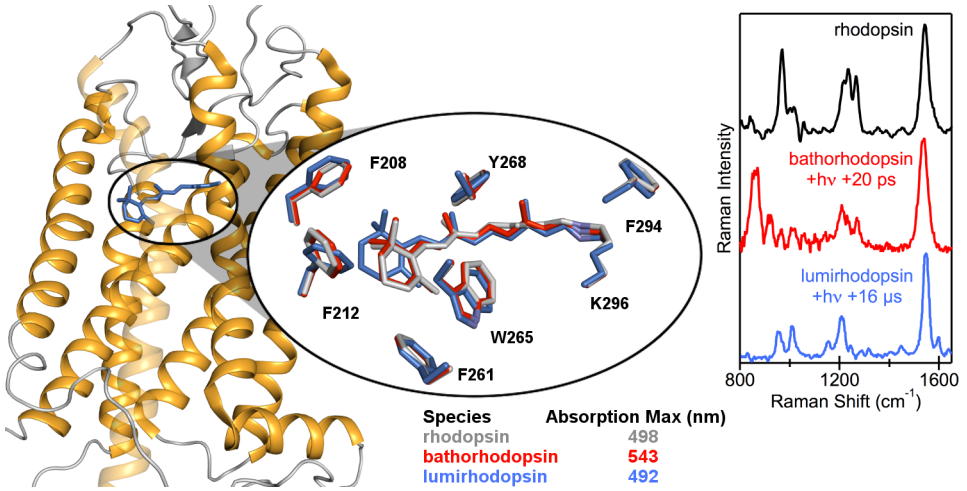

Figure 3. Crystal structures and resonance Raman spectra of rhodopsin (gray) and two photointermediates, bathorhodopsin (red) and lumirhodopsin (blue). The protein backbone is shown as yellow ribbons and corresponds to that of rhodopsin. Crystal structures are from Protein Data Bank entries 1U19 (rhodopsin), 2G87 (bathorhodopsin), and 2HPY (lumirhodopsin). Tryoptophan, tyrosine, and phenylalanine residues within 4.5 Å of the retinal chromophore are shown; Y178 has been omitted to preserve the unobstructed view of the binding pocket. Pump−probe time delays for resonance Raman spectra are indicated. Raman spectra are from refs 58 (rhodopsin and bathorhodopsin) and 60 (lumirhodopsin).

yields and high molar absorptivities of the reactants and photointermediates, rhodopsin and bacteriorhodopsin, as well as other retinal proteins, have been investigated extensively with resonance Raman spectroscopy.

The visual pigment rhodopsin, herein simply termed rhodopsin, is the protein responsible for vision in all vertebrates, mollusks, and arthropods. It is a well-studied G protein-coupled receptor (GPCR) and, in fact, was the first GPCR to be crystallized in 2000.[49] Early photochemical studies of mammalian rhodopsin were led by Wald and co-workers, who demonstrated in the early 1950s that the molecular basis of vision is the 11-*cis*-to-*trans* photoisomerization of a protein-bound retinal chromophore that absorbs maximally at 498 nm.[50] These and other foundational discoveries in vision were recognized by a Nobel Prize in 1967, and several years later, the first resonance Raman spectra of rhodopsin from intact bovine retinae[7] and solubilized in detergent[51] were reported.

The initial, groundbreaking resonance Raman studies were followed by a suite of rapid-flow, low-temperature, and pump−probe experiments that revealed the ground-state structures of rhodopsin and its photoproducts and thermal products. The first resonance Raman spectrum of the 77 K-trapped all-*trans* photoproduct,[52] called bathorhodopsin (λ_{max} = 543 nm), exhibited unusually intense peaks at 856, 877, and 920 cm^{-1} that were not present in resonance Raman spectra of the model compound, the all-*trans* protonated Schiff base. These resonance Raman and related transient absorption spectra led some to hypothesize that bathorhodopsin was not an all-*trans* species but instead reflected a *cis* structure that had undergone proton translocation[53] or tautomerization.[54] These hypotheses were shown to be incorrect, and subsequent low-temperature resonance Raman studies of isotopic derivatives led Mathies and co-workers to properly assign the intense bathorhodopsin peaks to hydrogen-out-of-plane (HOOP) modes of a highly strained and distorted all-*trans* chromophore.[55,56] Resonance Raman spectroscopy was key in establishing that the bathorhodopsin all-*trans* retinal chromophore is not planar, but instead, exhibits ∼40° dihedral twists about the C_{11}═C_{12} and C_{12}−C_{13} bonds because of protein−chromophore interactions.[57] This distorted photoproduct also exists at room temperature and appears within hundreds of femtoseconds following photon absorption.[58] The relevance of this distorted chromophore in bathorhodopsin has been the subject of many papers. It is now well accepted that a significant fraction of the photon energy is stored in these distortions, and that this strained chromophore ultimately drives global protein conformational changes for G protein activation.[57]

Other intermediates have also been investigated in detail with both low- and room-temperature resonance Raman spectroscopy; the room-temperature measurements were performed with time-resolved methods, such as fast-flow and pump−probe spectroscopy. Bathorhodopsin converts to the blue-shifted intermediate (BSI, λ_{max} of 477 nm), and this conversion is accompanied by partial relaxation in the all-*trans* structure.[59] The chromophore continues to relax and transfer energy to the surrounding protein as BSI decays to lumirhodopsin (λ_{max} = 492 nm), followed by Meta I (λ_{max} = 478 nm).[60] This relaxation is evident in the comparison of the resonance Raman spectra of rhodopsin,[58] bathorhodopsin,[58] and lumirhodopsin[60] in Figure 3; the intense, ∼850 cm^{-1} HOOP modes appear in bathorhodopsin but are absent in rhodopsin and lumirhodopsin. A comparison of the protein and chromophore structures based on X-ray diffraction highlights the surprising similarity between the 11-*cis* (rhodopsin) and distorted all-*trans* (bathorhodopsin) species and shows the subsequent structural changes in the relaxed lumirhodopsin form (Figure 3). This analysis of rhodopsin and bathorhodopsin illustrates that resonance Raman spectra of two species may exhibit significant differences despite relatively minor variations in crystallographic structures. Meta I decays to Meta II (λ_{max} = 380 nm), which exhibits a deprotonated all-*trans* retinal; Meta II is the signaling state of rhodopsin during which the G protein, transducin, is activated to initiate the enzymatic cascade. Finally, the retinal chromophore is released to yield the apoprotein opsin and all-*trans* retinal.

Our understanding of the chromophore dynamics as well as the global protein response associated with the isomerization reaction has been enhanced through time-resolved resonance Raman experiments. Picosecond visible pump−probe and femtosecond stimulated Raman spectroscopy (FSRS) experi-

DOI: 10.1021/acs.biochem.5b00514
Biochemistry 2015, 54, 4770−4783

ments demonstrated that the highly strained, all-*trans* chromophore of bathorhodopsin is present within 200 fs following photon absorption;[58,61] this time scale was consistent with transient absorption data[62] that had been reported at least 10 years prior to these resonance Raman studies. Analysis of the FSRS data further indicated that the photoproduct approaches its equilibrium structure in ~140 fs,[63] and picosecond anti-Stokes experiments revealed vibrational cooling of the chromophore in ~3 ps.[64] Transfer of the photon energy from the distorted chromophore to surrounding protein binding pocket has also been investigated with time-resolved UVRR spectroscopy (see below).

4. ULTRAVIOLET RESONANCE RAMAN (UVRR) SPECTROSCOPY

4.1. Protein Chromophores Investigated by UVRR. UV lasers have extended the application of resonance Raman spectroscopy to chromophores that absorb UV light and are prevalent in all proteins, such as amide backbone, aromatic amino acids, proline, and, to a lesser extent, sulfur-containing residues.[65,66] As was demonstrated for visible resonance Raman spectroscopy, selectivity in UVRR is also achieved by tuning the excitation wavelength. For example, the backbone carbonyl $\pi \rightarrow \pi^*$ transition is intense at wavelengths below ~210 nm, so excitation near 200 nm preferentially probes secondary structure. On the other hand, higher-wavelength excitation (~230 nm) probes side-chain structure. This selectivity is illustrated in the UVRR spectra of the peptide melittin, which has the primary sequence GIGAVLKVLTTGLPALISWIKRK-RQQ. Figure 4 shows that 210 nm excitation of melittin gives

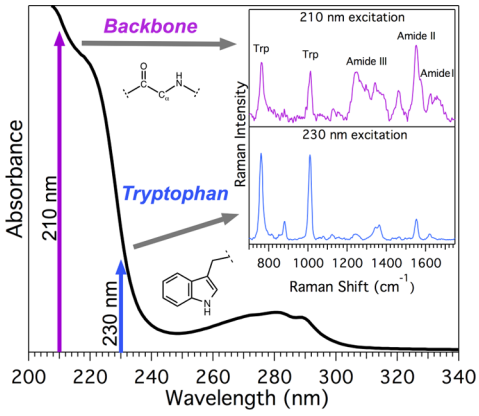

Figure 4. UVRR spectra of melittin in random coil conformation in buffer. The excitation wavelength is primarily resonant with the backbone (210 nm) or the single tryptophan residue at position 19 (230 nm). Modes that are enhanced with 210 nm are indicated in the top spectrum.

rise to a UVRR spectrum of the backbone that is different from that of the 230 nm spectrum of the single tryptophan residue at position 19.

4.1.1. Secondary Structure. The UVRR spectrum of amide backbone can be used to characterize secondary structure because of the sensitivity of vibrational frequencies to the hydrogen bonding environment. Intense UVRR bands appear for vibrations that involve carbonyl and amide functional groups: amide I (predominantly C═O stretch), amide II (~60% N−H bend + ~40% C−N stretch), and amide III (~40% C−N stretch + ~30% N−H bend) modes.[67] In addition to these well-known amide modes, the amide IIp mode of proline and the amide S mode are also utilized in UVRR spectroscopy.[66,68,69] Analysis of the amide III (~1250−1350 cm^{-1}), amide II (~1520−1560 cm^{-1}), amide I (~1630−1680 cm^{-1}), and amide S (~1390 cm^{-1}) regions reveals the relative content of random coil, α-helix, and β-sheet secondary structure in proteins and peptides.[68,70,71] A summary of vibrational normal modes and their correlation to structure and environment in UVRR spectra of proteins is presented in Table 1.

The information gained from UVRR analysis of the backbone may be compared to results from far-UV (190−250 nm) circular dichroism (CD) measurements. Because normal-mode frequencies may reflect variations in backbone dihedral angles, UVRR can report on a single turn of an α-helix.[72] In contrast, CD reports on the global average of the secondary structure of the peptide because of the effects of exciton coupling.[73] A consequence of this difference is that UVRR intensities scale linearly with the fraction of α-helix whereas in CD spectroscopy, the molar ellipticity per residue decreases as α-helical content decreases, and a threshold length of α-helix must persist to give reliable results in a CD spectrum.[74] Exciton coupling is especially important in CD spectra of short peptides. Short α-helical peptides result in CD spectra with variations in peak positions and relative intensities.[75] An additional challenge inherent to CD spectroscopy is that highly scattering samples are difficult to investigate. Differential light scattering and absorption flattening from particles, such as membrane vesicles, may alter the observed shapes and relative intensities in CD spectra.[76] Finally, CD spectra are broad and generally featureless relative to UVRR spectra and, therefore, do not easily reveal fractional contributions of mixed $\alpha-\beta$ sheet secondary structures. In summary, UVRR is an attractive alternative to far-UV CD spectroscopy that will provide additional insights into the secondary structures of challenging systems.

4.1.2. Aromatic Amino Acids. The majority of UVRR studies of side chains focus on tryptophan, tyrosine, and histidine because these aromatic residues have strong Raman peaks that report on structure, environment, and protonation state (see Table 1).[77−87] Phenylalanine, like tyrosine and tryptophan, also exhibits strong resonance Raman peaks whose intensities depend on the absorption cross section at the Raman excitation wavelength. However, in contrast to tryptophan and tyrosine, the Raman peaks of phenylanine are poor reporters of microenvironment because their peak positions are unchanged in varied solvents.[66] Hence, the UVRR spectrum of phenylalanine is not commonly studied. Off-resonance Raman studies of tryptophan and tyrosine have also played a critical role in interpretation of UVRR spectra.[88−91] These and other Raman studies have established empirical relationships between Raman frequencies/intensities and molecular details, including hydrogen bond strength, microenvironment, static structure, cation−π interactions, and protonation state. Figure 5 shows UVRR spectra of model compounds of tryptophan (*N*-acetyl-L-tryptophan ethyl ester), tyrosine (*N*-acetyl-L-tyrosinamide), and phenylalanine (L-phenylalanine).

Tryptophan exhibits an intense absorption band in the UV, and has consequently been extensively studied by UVRR. Systematic analyses revealed spectral signatures of the indole ring that report on local hydrophobicity, the strength of the indole N−H hydrogen bond, and the $C_2-C_3-C_\beta-C_\alpha$ torsional

DOI: 10.1021/acs.biochem.5b00514
Biochemistry 2015, 54, 4770−4783

Table 1. UVRR Bands of the Protein Backbone and Residues from refs 65, 66, 81, 85, and 86[a]

chemical group	designation	description	Raman shift (cm^{-1})	properties
tryptophan	W1	benzene ring stretch	1620	environment polarity
tryptophan	W3	CC pyrrole stretch	1552	structure
tryptophan	W4	CH bend + NH bend	1494	H-bonding
tryptophan	W6	NCC stretch + NH bend	1435	H-bonding
tryptophan	W7 doublet	Fermi doublet	1360 and 1340	environment polarity, π-interactions
tryptophan	W8	CC stretch + NH bend	1307	H-bonding
tryptophan	W9, W10	CH bend + NH bend	1230−1250	H-bonding
tryptophan	W16	benzene ring breathing	1004	environment polarity
tryptophan	W17	NH bend	879	H-bonding
tryptophan	HOOP	hydrogen out-of-plane	770−820	π-interactions
tryptophan	W18	indole breathing	760	environment polarity, π interactions
tyrosine	Y8a	ring stretch	1617	H-bonding, protonation state
tyrosine	Y8b	ring stretch	1601	H-bonding, protonation state
tyrosine	Y7a′	CO stretch	1263	proton-accepting strength
tyrosine	Y7a	CC stretch	1210	proton-donating strength
tyrosine	Y9a	CH bend + OH bend	1180	structure
tyrosine	Y1 + 2Y16a	Fermi doublet	850 and 830	H-bonding
histidine in D_2O	N/A	CC stretch and NCN stretch	1577 and 1317	neutral histidine
histidine-D^+ in D_2O	N/A	NCN stretch	1408	protonated histidine
amide backbone	amide I	CO stretch	1630−1680	secondary structure
amide backbone	amide II	CN stretch + NH bend	1520−1560	secondary structure
amide backbone	amide III	CN stretch + NH bend	1250−1350	secondary structure
amide backbone	amide S	CαH bend	1390	secondary structure
proline	amide IIp	CN stretch of X-Pro	1460	H-bonding, *cis*/*trans*

[a]Molecular and environment properties that are correlated to the band positions and intensities are also indicated. Designations and normal-mode descriptions that are not available are indicated N/A.

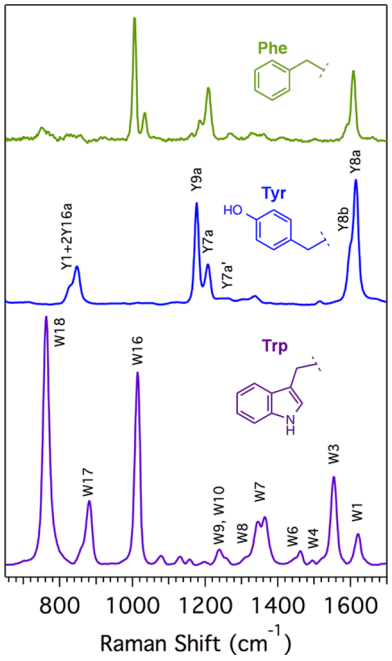

Figure 5. 230 nm UVRR spectra of L-phenylalanine (Phe), *N*-acetyl-L-tyrosinamide (Tyr), and *N*-acetyl-L-tryptophan ethyl ester (Trp). Amino acid side chains are shown. Labeled peaks correspond to those in Table 1.

angle, $\chi^{2,1}$. Although the near-UV (>250 nm) CD spectrum of tryptophan contains information about hydrophobicity and hydrogen bonding,[92] interpretation can be challenging because of broad and overlapping features of varying sign, and analysis should ideally be aided by UVRR.[93,94] Overall, the breadth of information in a UVRR spectrum of tryptophan makes this an excellent tool for a wide range of biophysical studies.

The ability of UVRR to report on tryptophan is advantageous because this amino acid is one of the most important residues in terms of protein structure, function, and dynamics. It is the least abundant residue in soluble proteins, accounting for only 1.1% of the amino acids expressed in cytoplasmic proteins,[95] but is more prevalent in membrane proteins, with an abundance of 2.9% in transmembrane α-helical domains.[96] This aromatic residue plays key functional roles in proteins because of its unique properties among the 20 natural amino acids: tryptophan exhibits the largest accessible nonpolar surface area that is polarizable, possesses an indole N−H moiety that is capable of hydrogen bond donation, and displays the greatest electrostatic potential for cation−π interactions.[97,98]

These important physical properties render tryptophan an ideal amphiphilic residue. As such, it displays the greatest propensity to reside in the interfacial region of membrane proteins compared to any other naturally occurring amino acid.[99] Tryptophan has been found to stabilize membrane-spanning proteins and peptides by acting as anchors along the interface of the bilayer.[100,101] Replacement of tryptophan residues with phenylalanine in the 325-residue integral membrane protein, outer membrane protein A, destabilizes the protein relative to the wild type when the protein is folded into lipid bilayers.[102,103] Tryptophan residues in membrane-associated antimicrobial peptides also play important functional roles in hemolytic and bactericidal activity.[104,105] These and other examples illustrate that the presence, location, and environment of tryptophan residues are critical in the study of folding and insertion of membrane proteins and membrane-associated peptides.

DOI: 10.1021/acs.biochem.5b00514
Biochemistry 2015, 54, 4770−4783

4.2. Applications of UVRR Spectroscopy to Proteins and Peptides. Soluble and membrane proteins have been investigated via UVRR. We briefly describe UVRR studies of soluble proteins and describe recent investigations of more challenging membrane-associated and aggregated proteins and peptides. The choice of biological systems that are discussed is intended to be representative of the array of biomolecules that may be studied as well as the types of scientific questions that may be investigated.

4.2.1. Soluble Proteins. A wide range of soluble proteins and scientific questions have been investigated via UVRR. UVRR frequencies and intensities are sensitive to environment, so it is relatively straightforward to correlate UVRR peaks with the local environment of tryptophan and tyrosine residues in proteins, including interactions with metals and charged residues.[80,88,106−111] One advantage of UVRR over electronic tools, such as fluorescence, is that the effects of hydrogen bonding and local dielectric on UVRR peaks are separable, thereby allowing independent investigations of changes in H-bonding or hydrophobicity.[81] Histidine protonation states are easily determined by UVRR studies of protein in D_2O buffer, and such experiments have been performed on superoxide dismutase and galectins.[112−114] An area with growing use of UVRR is the pharmaceutical industry, in which UVRR experiments have been reported for recombinant therapeutic proteins[115] and antibodies[116] as well as drug binding.[117,118] Time-resolved UVRR experiments have also probed dynamics of heme proteins and photoactive yellow protein,[119−122] and a variety of UVRR experiments have investigated intermediates in protein folding.[123,124] In addition to native side chains and the backbone, other moieties have been interrogated by UVRR, such as unnatural amino acids[125] and flavins.[126] These and other examples illustrate the breadth of information gained from UVRR studies of soluble proteins.

4.2.2. Membrane Proteins. Membrane proteins have also been investigated by UVRR, but these systems are more challenging to study than soluble proteins because of limited sample quantities and high background scattering from vesicles or micelles. Bacteriorhodopsin and rhodopsin are perhaps the most well-studied membrane proteins, with UVRR papers on bacteriorhodopsin first appearing nearly 25 years ago.[127,128] Since these initial reports, other steady-state and pump−probe UVRR experiments have elucidated changes in structure during the bacteriorhodopsin photocycle, such as modifications in local and hydrogen bonding environments of tyrosine and tryptophan residues, opening of a water-permeable channel, and the picosecond-to-nanosecond response of protein pocket to isomerization reaction.[129−135] Experiments on the visual pigment rhodopsin have also been reported.[34,136,137] The insights gained from these UVRR studies have revealed the response of the retinal binding pocket to photon absorption. For example, it has been shown that there is a 3 ps response of tryptophan and tyrosine residues to the photoisomerization reaction.[34] A small number of other detergent-solubilized membrane proteins have also been investigated, such as photosystem II,[138] cytochrome *c* oxidase,[139] and cytochrome bc_1 complex.[140] In the past several years, UVRR experiments have been extended to a membrane protein embedded in a synthetic lipid bilayer.[141,142] In particular, UVRR studies of outer membrane protein A (OmpA) and its mutants revealed tryptophan−lipid interactions during the insertion and folding of OmpA into bilayers of small unilamellar vesicles.[141,142] The ability to gain insight into the dynamics of membrane proteins is an important advantage of UVRR and allows for investigations of complex reactions and systems that may not be amenable to traditional tools such as NMR or crystallography.

4.2.3. Model Peptides for Soluble and Membrane Protein Folding. Small peptides provide an excellent opportunity to investigate protein folding. Model peptides are especially valuable for studies of membrane protein folding because experiments and data analysis can be simplified. Additionally, the expression and purification of large quantities of integral membrane proteins is a challenging task, whereas membrane-associated peptides can be synthesized in sufficient quantities. UVRR spectroscopy is well-suited for the study of membrane-associated biomolecules because the presence of lipid vesicles and detergents does not complicate the spectra.[142]

Several groups have measured UVRR spectra of small peptides to study the structures and kinetics of soluble protein folding. Asher and co-workers,[143] for example, have studied the kinetics and thermal stability of α-helix-like soluble peptides. In contrast, only a small number of model membrane peptides have been studied. One such model membrane peptide, *N*-acetyl-tryptophan-pentaleucine (AcWL5), was found to have β-sheet-type structure in lipid vesicles based on results obtained from UVRR spectra;[144] this finding is in accordance with the β-sheet oligomeric structure previously reported for AcWL5.[145] The UVRR spectrum revealed that the tryptophan residue in AcWL5 is hydrogen-bonded in a hydrophobic region of the lipid bilayer. This result provides a molecular description of how tryptophan is able to help stabilize membrane proteins.[100] The hydrophobic α-helical model membrane peptide, ME1, has also been investigated using UVRR spectroscopy. ME1 is a 32-residue transmembrane helix segment of the natural membrane protein glycophorin A that has five additional mutations. Comparison of the UVRR spectrum of this peptide to that of the soluble α-helical protein myoglobin led to the conclusion that the intensity of UVRR amide bands serves as a reliable marker to identify lipid-solubilized and solvent-exposed helical structure in proteins.[146] A final example of a membrane-associated peptide for folding studies is the α-helical, pH low insertion peptide (pHLIP). This peptide exhibits structural changes as a function of pH, and UVRR experiments determined that this peptide is desolvated and structured as a membrane-associated peptide.[147]

4.2.4. Antimicrobial Peptides (AMPs). While the membrane peptides described above serve as model systems for protein folding, some small membrane-active peptides fold and insert into lipid bilayers and function as membrane disruptors. One such class of peptides is antimicrobial peptides (AMPs). AMPs are an ancient component of innate immunity that are selectively toxic to bacteria[148] and are crucial for the survival of many organisms that do not possess lymphocytes or antibodies important for immunity, such as insects.[149] AMPs typically have fewer than 50 residues and generally exhibit segregated regions of cationic and hydrophobic amino acid residues that give rise to an amphiphilic structure for binding to membranes.[149] In the presence of a bilayer, they form α-helices or rigid β-sheet structures with disulfide bridges and often exhibit primary sequences with an unusually high abundance of select amino acids.[148,150] Mutation or deletion of certain residues, including tryptophan, has been found to be detrimental to the activity of many AMPs.[104,151−153] These peptides are water-soluble yet spontaneously insert into membranes and, therefore, have properties of both soluble

DOI: 10.1021/acs.biochem.5b00514
Biochemistry 2015, 54, 4770−4783

and membrane proteins. The observation that bacteria do not develop resistance to AMPs suggests that AMPs may serve as a novel class of antibiotics to combat antibiotic-resistant bacteria. This potentially transformative use of AMPs motivates UVRR and other studies of the mechanisms of membrane disruption.

The mechanisms of AMP insertion and folding into membranes are not well understood. Electrostatic interaction between cationic AMPs and anionic bacterial membranes is important for initial peptide−membrane binding. However, the formation of salt bridges does not fully explain the selectivity of AMPs for bacterial over eukaryotic membranes. Several models of AMP disruption mechanisms have been proposed. In one model, AMPs carpet the membrane, causing an increase in the permeability of the membrane. AMPs may form pores that cause ions and molecules to leak out through the membrane. It has also been proposed that AMPs simply act to dissolve the membrane in a manner similar to that of a detergent.[148]

One example of an AMP that has been successfully studied by UVRR is the human cathelicidin, LL-37.[154] This AMP is expressed primarily in neutrophils and epithelial cells and shows broad-spectrum antimicrobial activity.[155] An important goal of this project was to elucidate the microenvironment of the peptide buried in a bilayer and thus shed light on the mechanisms of membrane disruption. In this study, phenylalanine residues at positions 6 and 17 were replaced with tryptophan residues and yielded the two single-tryptophan mutant peptides F6W and F17W. These mutations did not alter the antimicrobial activity or the overall secondary structure compared to those of wild-type peptide LL-37. On the basis of results obtained from fluorescence quenching experiments and UVRR spectroscopy, the positions of tryptophan residues for both mutants were found to be deeply buried in the lipid bilayer (∼12 Å from the bilayer center) of mixed anionic/zwitterionic lipid vesicles (bacterial membrane mimics). UVRR data revealed a decrease in hydrogen bonding and environment polarity for both tryptophan residues upon folding and insertion of the peptide into the lipid bilayer; this finding is consistent with deep insertion of the aromatic residues into the bilayer. The UVRR results, combined with fluorescence and CD data, ruled out a detergent-like mode of action for this AMP and, instead, supported carpeting and/or toroidal pore mechanisms.

The UVRR and fluorescence results complement previous NMR studies by Ramamoorthy and colleagues.[156] Both studies support the possible mechanisms of carpeting and/or toroidal pore and suggest that the orientation of LL-37 in the bilayer is parallel, not perpendicular, to the bilayer surface. The solid-state NMR experiments also suggested that LL-37 lies at the bilayer surface and is immobilized. One of the strengths of UVRR is the ability to reveal microscopic detail near the tryptophan residue without the need for isotopic labeling or high concentrations typical of NMR studies. The UVRR results suggest that tryptophan is not interacting with lipid headgroups but, instead, is likely buried in the hydrocarbon core of the bilayer. Analysis of the W18 and W16 tryptophan modes suggests that possible intramolecular cation−π interactions may stabilize one of the buried tryptophan residues in the bilayer. UVRR data also directly reveal differences in the level of hydration among random coil, soluble oligomer, and vesicle-bound forms of LL-37. Collectively, these molecular insights augment structural information that is gained through NMR studies and deepen our understanding of LL-37.

The AMPs lactoferricin B (LfB) and pEM-2 have also been investigated using UVRR spectroscopy.[157] LfB is an α-helical 25-residue peptide composed of a segment of bovine lactoferrin, and pEM-2 is a modified 13-residue peptide derived from myotoxin isolated from *Bothrops asper* snake venom. Both peptides have tryptophan residues that are important for AMP activity against Gram-negative and -positive bacteria.[158,159] As revealed by UVRR experiments, the hydrophobicity of tryptophan environments increased when both peptides were introduced into the helix-inducing solvent 2,2,2-trifluoroethanol. Additionally, the hydrophobicity near the tryptophan residues of LfB did not increase in the presence of purely zwitterionic lipid vesicles (eukaryotic membrane mimic). However, the hydrophobicity was enhanced in the presence of anionic lipid vesicles (bacterial membrane mimic), indicating that LfB preferentially folds and inserts into lipid bilayers that mimic bacterial membranes.

Similar results were found for the anoplin peptide, an α-helical peptide isolated from the venom of the wasp *Anthemis samariensis*.[160] Modifications in the primary structure of the peptide, including full substitutions of L-amino acids for D-amino acids and C-terminal deamidation, did not change the overall secondary structure of the peptide based on the results obtained with UVRR spectroscopy. Furthermore, it was found that all modified forms of the peptide adopted α-helical secondary structure in the presence of anionic lipid vesicles. Very little peptide structure was observed in the presence of zwitterionic lipid vesicles, further confirming the preferential binding of AMPs for anionic synthetic lipid bilayers.

A final example that illustrates the utility of UVRR experiments is the chimeric peptide CM15, which is a hybrid peptide comprised of seven residues from the AMP cecropin (from silk moth) and eight residues from the toxic peptide melittin (from honeybee venom).[161] CM15 is engineered to combine the best of two worlds: it is potent, like melittin, but selective and nonhemolytic, like cecropin. UVRR analysis of CM15 with both 228 and 210 nm excitation led to the surprising result that unlike typical AMPs and toxins, CM15 retains a predominantly unfolded, hydrated, conformation when bound to vesicles comprised of zwitterionic lipids. Even more unexpected was the finding that this unfolded CM15 is a potent membrane disruptor as assessed by fluorescence leakage assays. UVRR spectra of melittin, cecropin, and the hybrid CM15 in three different environments are shown in Figure 6; all three peptides are unfolded in buffer and fully folded as α-helices in the presence of anionic lipid vesicles. The fraction of α-helix in the presence of zwitterionic lipids was determined by using the unfolded and fully folded spectra as basis spectra. CM15 was found to be only 23% α-helical when bound to zwitterionic vesicles, but it was nearly as potent as melittin (89% α-helical) in terms of membrane disruption. This finding that an engineered, hybrid peptide exhibits high potency as an unfolded peptide suggests that new models for peptide−membrane interactions may be needed.[161]

4.2.5. Fibril-Forming Peptides. Another family of challenging biomolecules consists of the aggregation-prone disordered peptides. Amyloid-β (Aβ) is an intrinsically unstructured peptide (29−43 amino acids) derived from proteolysis of the larger Aβ precursor protein. For reasons that are not yet understood, Aβ forms well-ordered insoluble aggregates, or fibrils, that collect as plaques in the brains of Alzheimer's patients. Because of the unique properties of this peptide, techniques typically utilized to elucidate protein structure, such

DOI: 10.1021/acs.biochem.5b00514
Biochemistry 2015, 54, 4770−4783

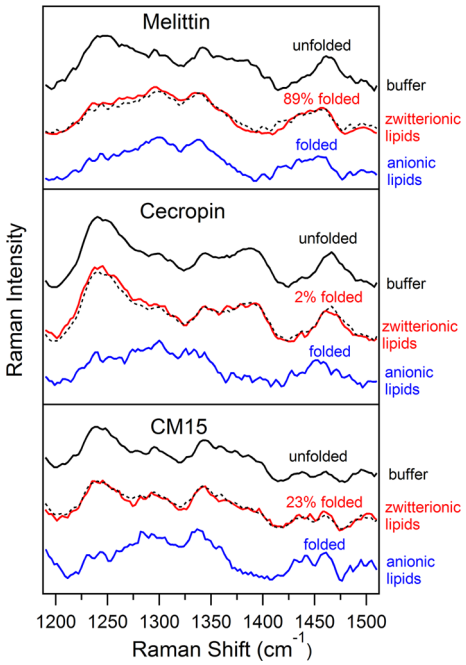

Figure 6. 210 nm UVRR spectra of melittin, cecropin, and CM15 in three different environments of buffer (fully unfolded), zwitterionic lipid vesicles (partially folded), and anionic lipid vesicles (fully folded). Fraction folded in zwitterionic lipids was determined by linear combination of fully folded and unfolded spectra, and best fits are shown as black dashed curves that overlay red curves. Resulting fractions are indicated. This figure is adapted from ref 161. See the text for details.

as X-ray crystallography and solution NMR, are not well-suited for studying the structures of the biologically relevant, unfolded forms of this peptide.[162] UVRR spectroscopy, however, does not require a crystalline or homogeneous phase and, therefore, can be used to elucidate structures of disordered peptides and proteins, including fibrils and heterogeneous aggregates. An additional benefit is that UVRR spectroscopy specifically reports on hydrogen bonding networks that give rise to peptide secondary structure, local hydrophobicity, and tertiary contacts that are known to be associated with aggregate formation.[163,164] In the context of these advantages, UVRR spectroscopy, in particular deep UV (<200 nm excitation), is ideally suited for the study of Aβ and other peptides that may be linked to neurodegenerative disorders.

A relatively small number of UVRR studies of Aβ peptides have been published. The deep UVRR spectra of Aβ peptides that form either parallel or antiparallel β-sheets have been characterized. It was reported that these different β-sheet motifs of amyloid fibrils could be distinguished via UVRR.[165] This study further indicated that the parallel β-sheet conformation in fibrils is different from the analogous β-sheets in soluble proteins. In contrast, antiparallel β-sheet conformations were described to be similar for both fibrils and soluble proteins. In another study, myricetin, a flavenoid known to interact with Aβ, was observed to inhibit amyloid formation of Aβ via a thioflavin T assay. Additionally, results from CD and UVRR experiments revealed that myricetin altered the conformation of the hydrophobic segment of the peptide and may interact with the aromatic amino acids present in Aβ. This finding indicates that UVRR spectroscopy may be sensitive to changes in peptide structure when anti-amyloidogenic small molecules are introduced into the sample.[166] These important discoveries on the structure of Aβ in amyloid fibrils underscore the flexibility of UVRR spectroscopy and the level of molecular detail that can be attained by this technique.

5. CONCLUSION

Resonance Raman spectroscopy is a valuable optical technique that elucidates structures and dynamics of biomolecules. A primary advantage of this method over other vibrational and structural tools is the ability to interrogate select portions of the protein by tuning the excitation wavelength to within an absorption band of the chromophore of interest. Given the widespread availability of robust and tunable UV-to-visible lasers, it is now relatively straightforward to obtain resonance Raman spectra of the protein backbone, side chains, and colored prosthetic groups. In combination with modern pulsed methods, resonance Raman spectroscopy is able to reveal structural changes and functional dynamics of biomolecules over all relevant time scales, from femtoseconds to seconds. These benefits make resonance Raman spectroscopy an excellent complement to the many other tools used in the study of the most complex and experimentally challenging biomolecules.

AUTHOR INFORMATION

Corresponding Author

*Phone: 858-534-8080. Fax: 858-534-7042. E-mail: judyk@ucsd.edu.

Funding

I.L.-P. acknowledges generous support from a UCSD National Institutes of Health Molecular Biophysics Training Grant Fellowship and a Department of Education Graduate Assistance in Areas of National Need (GAANN) Fellowship. We acknowledge the National Science Foundation for supporting our research program.

Notes

The authors declare no competing financial interest.

ACKNOWLEDGMENTS

We thank Prof. Michael Tauber for valuable feedback.

REFERENCES

(1) Raman, C. V., and Krishnan, K. S. (1928) A new type of secondary radiation. *Nature 121*, 501−502.
(2) Singh, R. (2002) C. V. Raman and the discovery of the Raman effect. *Phys. Perspect. 4*, 399−420.
(3) McCreery, R. L. (2000) *Raman Spectroscopy for Chemical Analysis*, Wiley Interscience, New York.
(4) Merlin, J. C. (1985) Resonance Raman spectroscopy of carotenoids and carotenoid-containing systems. *Pure Appl. Chem. 57*, 785−792.
(5) Carey, P. R. (1982) *Biochemical Applications of Raman and Resonance Raman Spectroscopies*, Academic Press, New York.
(6) Myers, A. B., and Mathies, R. A. (1984) Resonance Raman Intensities: A Probe of Excited-State Structure and Dynamics. In *Biological Applications of Raman Spectroscopy* (Spiro, T. G., Ed.) pp 1−58, John Wiley and Sons, Inc., New York.
(7) Rimai, L., Kilponen, R. G., and Gill, D. (1970) Resonance-enhanced Raman spectra of visual pigments in intact bovine retinas at low temperatures. *Biochem. Biophys. Res. Commun. 41*, 492−497.
(8) Gill, D., Kilponen, R. G., and Rimai, L. (1970) Resonance Raman scattering of laser radiation by vibrational modes of carotenoid pigment molecules in intact plant tissues. *Nature 227*, 743−744.

DOI: 10.1021/acs.biochem.5b00514
Biochemistry 2015, 54, 4770−4783

(9) Strekas, T. C., and Spiro, T. G. (1972) Hemoglobin: Resonance Raman spectra. *Biochim. Biophys. Acta, Protein Struct. 263*, 830−833.
(10) Brunner, H., Mayer, A., and Sussner, H. (1972) Resonance Raman scattering on the haem group of oxy- and deoxyhaemoglobin. *J. Mol. Biol. 70*, 153−156.
(11) Strekas, T. C., and Spiro, T. G. (1972) Cytochrome *c*: Resonance Raman spectra. *Biochim. Biophys. Acta, Protein Struct. 278*, 188−192.
(12) Warshel, A. (1977) Interpretation of resonance Raman spectra of biological molecules. *Annu. Rev. Biophys. Bioeng. 6*, 273−300.
(13) Deng, H., and Callender, R. (1999) Raman spectroscopic studies of the structures, energetics, and bond distortions of substrates bound to enzymes. *Methods Enzymol. 308*, 176−201.
(14) Moffat, K. (2001) Time-resolved biochemical crystallography: A mechanistic perspective. *Chem. Rev. 101*, 1569−1581.
(15) Gardner, K. H., and Kay, L. E. (1998) The use of H-2, C-13, N-15 multidimensional NMR to study the structure and dynamics of proteins. *Annu. Rev. Biophys. Biomol. Struct. 27*, 357−406.
(16) Terner, J., Spiro, T. G., Nagumo, M., Nicol, M. F., and El-Sayed, M. A. (1980) Resonance Raman spectroscopy in the picosecond time scale: The carboxyhemoglobin photointermediate. *J. Am. Chem. Soc. 102*, 3238−3239.
(17) Hayward, G., Carlsen, W., Siegman, A., and Stryer, L. (1981) Retina chromophore of rhodopsin photoisomerizes within picoseconds. *Science 211*, 942−944.
(18) Doig, S. J., Reid, P. J., and Mathies, R. A. (1991) Picosecond time-resolved resonance Raman spectroscopy of bacteriorhodopsin's J, K, and KL intermediates. *J. Phys. Chem. 95*, 6372−6379.
(19) Petrich, J. W., Martin, J. L., Houde, D., and Orszag, A. (1987) Time-resolved Raman spectroscopy with subpicosecond resolution: Vibrational cooling and delocalization of strain energy in photodissociated (carbonmonoxy)hemoglobin. *Biochemistry 26*, 7914−7923.
(20) Gustafson, T. L., Roberts, D. M., and Chernoff, D. A. (1983) Picosecond transient Raman spectroscopy: The photoisomerization of trans-stilbene. *J. Chem. Phys. 79*, 1559−1564.
(21) Uesugi, Y., Mizutani, Y., and Kitagawa, T. (1997) Developments of widely tunable light sources for picosecond time-resolved resonance Raman spectroscopy. *Rev. Sci. Instrum. 68*, 4001−4008.
(22) Zhu, L., Kim, J., and Mathies, R. A. (1999) Picosecond time-resolved Raman system for studying photochemical reaction dynamics to the primary events in vision. *J. Raman Spectrosc. 30*, 777−783.
(23) Kruglik, S. G., Lambry, J. C., Martin, J. L., Vos, M. H., and Negrerie, M. (2011) Sub-picosecond Raman spectrometer for time-resolved studies of structural dynamics in heme proteins. *J. Raman Spectrosc. 42*, 265−275.
(24) McCamant, D. W., Kukura, P., and Mathies, R. A. (2003) Femtosecond time-resolved stimulated Raman spectroscopy: Application to the ultrafast internal conversion in *β*-carotene. *J. Phys. Chem. A 107*, 8208−8214.
(25) Kukura, P., McCamant, D. W., and Mathies, R. A. (2007) Femtosecond stimulated Raman spectroscopy. *Annu. Rev. Phys. Chem. 58*, 461−488.
(26) Yoshizawa, M., Hattori, Y., and Kobayashi, T. (1994) Femtosecond time-resolved resonance Raman gain spectroscopy in polydiacetylene. *Phys. Rev. B: Condens. Matter Mater. Phys. 49*, 13259−13262.
(27) Laimgruber, S., Schreier, W. J., Schrader, T., Koller, F., Zinth, W., and Gilch, P. (2005) The photochemistry of *o*-nitrobenzaldehyde as seen by femtosecond vibrational spectroscopy. *Angew. Chem., Int. Ed. 44*, 7901−7904.
(28) Pézolet, M., Yu, T. J., and Peticolas, W. L. (1975) Resonance and preresonance Raman spectra of nucleotides using ultraviolet lasers. *J. Raman Spectrosc. 3*, 55−64.
(29) Hirakawa, A. Y., and Tsuboi, M. (1975) Molecular geometry in an excited electronic state and a preresonance Raman effect. *Science 188*, 359−361.
(30) Ziegler, L. D., and Albrecht, A. C. (1979) Ultraviolet preresonance Raman scattering of benzene derivatives. I. Excitation profiles for fundamentals. *J. Chem. Phys. 70*, 2634−2643.
(31) Balakrishnan, G., Hu, Y., Nielsen, S. N., and Spiro, T. G. (2005) Tunable kHz deep ultraviolet (193-210 nm) Laser for Raman applications. *Appl. Spectrosc. 59*, 776−781.
(32) Bykov, S., Lednev, I., Ianoul, A., Mikhonin, A., Munro, C., and Asher, S. A. (2005) Steady-state and transient ultraviolet resonance Raman spectrometer for the 193−270 nm spectral region. *Appl. Spectrosc. 59*, 1541−1552.
(33) Lednev, I. K., Ermolenkov, V. V., He, W., and Xu, M. (2005) Deep-UV Raman spectrometer tunable between 193 and 205 nm for structural characterization of proteins. *Anal. Bioanal. Chem. 381*, 431−437.
(34) Kim, J. E., Pan, D., and Mathies, R. A. (2003) Picosecond dynamics of G-protein coupled receptor activation in rhodopsin from time-resolved UV resonance Raman spectroscopy. *Biochemistry 42*, 5169−5175.
(35) Zhao, X., Chen, R., Tengroth, C., and Spiro, T. G. (1999) Solid-state tunable kHz ultraviolet laser for Raman applications. *Appl. Spectrosc. 53*, 1200−1205.
(36) Kaminaka, S., and Mathies, R. A. (1998) High-throughput large-aperture prism prefilter for ultraviolet resonance Raman spectroscopy. *Appl. Spectrosc. 52*, 469−473.
(37) Hashimoto, S., Ikeda, T., Takeuchi, H., and Harada, I. (1993) Utilization of a prism monochromator as a sharp-cut band-pass filter in ultraviolet Raman spectroscopy. *Appl. Spectrosc. 47*, 1283−1285.
(38) Russell, M. P., Vohnik, S., and Thomas, G. J., Jr. (1995) Design and performance of an ultraviolet resonance Raman spectrometer for proteins and nucleic acids. *Biophys. J. 68*, 1607−1612.
(39) Kaminaka, S., and Kitagawa, T. (1992) A novel idea for practical UV resonance Raman measurement with a double monochromator and its application to protein structural studies. *Appl. Spectrosc. 46*, 1804−1808.
(40) Trulson, M. O., Lueck, H. B., and Friedrich, D. M. (1994) Performance of a spatial-filter-equipped single monochromator for Raman spectroscopy. *Appl. Spectrosc. 48*, 720−723.
(41) McFarland, J. T. (1987) Flavins. In *Biological Applications of Raman Spectroscopy: Volume 2* (Spiro, T. G., Ed.) pp 211−301, John Wiley and Sons, Inc., New York.
(42) McCamant, D. W., Kukura, P., and Mathies, R. A. (2003) Femtosecond broadband stimulated Raman: A new approach for high-performance vibrational spectroscopy. *Appl. Spectrosc. 57*, 1317−1323.
(43) Cherepy, N. J., Shreve, A. P., Moore, L. J., Boxer, S. G., and Mathies, R. A. (1997) Temperature dependence of the Q(y) resonance Raman spectra of bacteriochlorophylls, the primary electron donor, and bacteriopheophytins in the bacterial photosynthetic reaction center. *Biochemistry 36*, 8559−8566.
(44) Matousek, P., Towrie, M., Stanley, A., and Parker, A. W. (1999) Efficient rejection of fluorescence from Raman spectra using picosecond Kerr gating. *Appl. Spectrosc. 53*, 1485−1489.
(45) Efremov, E. V., Buijs, J. B., Gooijer, C., and Ariese, F. (2007) Fluorescence rejection in resonance Raman spectroscopy using a picosecond-gated intensified charge-coupled device camera. *Appl. Spectrosc. 61*, 571−578.
(46) Shreve, A. P., Cherepy, N. J., and Mathies, R. A. (1992) Effective rejection of fluorescence interference in Raman spectroscopy using a shifted excitation difference technique. *Appl. Spectrosc. 46*, 707−711.
(47) Fang, C., Frontiera, R. R., Tran, R., and Mathies, R. A. (2009) Mapping GFP structure evolution during proton transfer with femtosecond Raman spectroscopy. *Nature 462*, 200−205.
(48) Ernst, O. P., Lodowski, D. T., Elstner, M., Hegemann, P., Brown, L. S., and Kandori, H. (2014) Microbial and animal rhodopsins: Structures, functions, and molecular mechanisms. *Chem. Rev. 114*, 126−163.
(49) Palczewski, K., Kumasaka, T., Hori, T., Behnke, C. A., Motoshima, H., Fox, B. A., Trong, I. S., Teller, D. C., Okada, T., Stenkamp, R. E., Yamamoto, M., and Miyano, M. (2000) Crystal structure of rhodopsin: A G protein-coupled receptor. *Science 289*, 739−745.
(50) Wald, G. (1968) Molecular basis of visual excitation. *Science 162*, 230−239.

DOI: 10.1021/acs.biochem.5b00514
Biochemistry 2015, 54, 4770−4783

(51) Lewis, A., Fager, R. S., and Abrahamson, E. W. (1973) Tunable laser resonance Raman spectroscopy of the visual process. *J. Raman Spectrosc. 1*, 465−470.
(52) Oseroff, A. R., and Callender, R. H. (1974) Resonance Raman spectroscopy of rhodopsin in retinal disk membranes. *Biochemistry 13*, 4243−4248.
(53) Peters, K., Applebury, M. L., and Rentzepis, P. M. (1977) Primary photochemical event in vision: Proton translocation. *Proc. Natl. Acad. Sci. U. S. A. 74*, 3119−3123.
(54) Fransen, M. R., Luyten, W. C. M. M., van Thuijl, J., Lugtenburg, J., Jansen, P. A. A., van Breugel, P. J. G. M., and Daemen, F. J. M. (1976) Structure of the chromophoric group in bathorhodopsin. *Nature 260*, 726−727.
(55) Eyring, G., Curry, B., Mathies, R., Fransen, R., Palings, I., and Lugtenburg, J. (1980) Interpretation of the resonance Raman spectrum of bathrhodopsin based on visual pigment analogues. *Biochemistry 19*, 2410−2418.
(56) Palings, I., Van den Berg, E. M. M., Lugtenburg, J., and Mathies, R. A. (1989) Complete assignment of the hydrogen-out-of-plane wagging vibrations of bathrhodopsin: Chromophore structure and energy storage in the primary photoproduct of vision. *Biochemistry 28*, 1498−1507.
(57) Yan, E. C. Y., Ganim, Z., Kazmi, M. A., Chang, B. S. W., Sakmar, T. P., and Mathies, R. A. (2004) Resonance Raman analysis of the mechanism of energy storage and chromophore distortion in the primary visual photoproduct. *Biochemistry 43*, 10867−10876.
(58) Kim, J. E., McCamant, D. W., Zhu, L., and Mathies, R. A. (2001) Resonance Raman structural evidence that the cis-to-trans isomerization in rhodopsin occurs in femtoseconds. *J. Phys. Chem. B 105*, 1240−1249.
(59) Pan, D., Ganim, Z., Kim, J. E., Verhoeven, M. A., Lugtenburg, J., and Mathies, R. A. (2002) Time-resolved resonance Raman analysis of chromophore structural changes in the formation and decay of rhodopsin's BSI intermediate. *J. Am. Chem. Soc. 124*, 4857−4864.
(60) Pan, D., and Mathies, R. A. (2001) Chromophore structure in lumirhodopsin and metarhodopsin I by time-resolved resonance Raman microchip spectroscopy. *Biochemistry 40*, 7929−7936.
(61) Kukura, P., McCamant, D. W., Yoon, S., Wandschneider, D. B., and Mathies, R. A. (2005) Structural observation of the primary isomerization in vision with femtosecond-stimulated Raman. *Science 310*, 1006−1009.
(62) Schoenlein, R. W., Peteanu, L. A., Mathies, R. A., and Shank, C. V. (1991) The first step in vision: Femtosecond isomerization of rhodopsin. *Science 254*, 412−415.
(63) McCamant, D. W. (2011) Re-evaluation of rhodopsin's relaxation kinetics determined from femtosecond stimulated Raman lineshapes. *J. Phys. Chem. B 115*, 9299−9305.
(64) Kim, J. E., and Mathies, R. A. (2002) Anti-Stokes Raman study of vibrational cooling dynamics in the primary photochemistry of rhodopsin. *J. Phys. Chem. A 106*, 8508−8515.
(65) Harada, I., and Takeuchi, H. (1986) Raman and Ultraviolet Resonance Raman Spectra of Proteins and Related Compounds. In *Spectroscopy of Biological Systems* (Clark, R. J. H., and Hester, R. E., Eds.) John Wiley & Sons, Ltd., Chichester, U.K.
(66) Austin, J. C., Jordan, T., and Spiro, T. G. (1993) Ultraviolet Resonance Raman Studies of Proteins and Related Model Compounds. In *Biomolecular Spectroscopy, Part A* (Clark, R. J. H., and Hester, R. E., Eds.) pp 55−127, John Wiley and Sons, New York.
(67) Cantor, C. R., and Schimmel, P. R. (1980) *Biophysical Chemistry*, W. H. Freeman and Company, New York.
(68) Wang, Y., Purrello, R., Jordan, T., and Spiro, T. G. (1991) UVRR spectroscopy of the peptide bond. 1. Amide S, a nonhelical structure marker, is a CαH bending mode. *J. Am. Chem. Soc. 113*, 6359−6368.
(69) Jordan, T., Mukerji, I., Wang, Y., and Spiro, T. G. (1996) UV resonance Raman spectroscopy and hydrogen bonding of the proline peptide bond. *J. Mol. Struct. 379*, 51−64.
(70) Huang, C.-Y., Balakrishnan, G., and Spiro, T. G. (2006) Protein secondary structure from deep-UV resonance Raman spectroscopy. *J. Raman Spectrosc. 37*, 277−282.
(71) Chi, Z., Chen, X. G., Holtz, J. S. W., and Asher, S. A. (1998) UV resonance Raman-selective amide vibrational enhancement: quantitative methodology for determining protein secondary structure. *Biochemistry 37*, 2854−2864.
(72) Ozdemir, A., Lednev, I. K., and Asher, S. A. (2002) Comparison between UV Raman and circular dichroism detection of short α-helices in bombolitin III. *Biochemistry 41*, 1893−1896.
(73) Sreerama, N., and Woody, R. W. (2000) *Circular Dichroism of Peptides and Proteins*, John Wiley and Sons, Hoboken, NJ.
(74) Woody, R. W. (1996) *Theory of Circular Dichroism of Proteins*, Plenum Press, New York.
(75) Chin, D. H., Woody, R. W., Rohl, C. A., and Baldwin, R. L. (2002) Circular dichroism spectra of short, fixed-nucleus alanine helices. *Proc. Natl. Acad. Sci. U. S. A. 99*, 15416−15421.
(76) Wallace, B. A., Lees, J. G., Orry, A. J. W., Lobley, A., and Janes, R. W. (2003) Analyses of circular dichroism spectra of membrane proteins. *Protein Sci. 12*, 875−884.
(77) Fodor, S. P. A., Copeland, R. A., Grygon, C. A., and Spiro, T. G. (1989) Deep-ultraviolet Raman excitation profiles and vibronic scattering mechanisms of pheylalanine, tyrosine, and tryptophan. *J. Am. Chem. Soc. 111*, 5509−5518.
(78) Sweeney, J. A., and Asher, S. A. (1990) Tryptophan UV resonance Raman excitation profiles. *J. Phys. Chem. 94*, 4784−4791.
(79) Chi, Z., and Asher, S. A. (1998) UV Raman determination of the environment and solvent exposure of tyr and trp residues. *J. Phys. Chem. B 102*, 9595−9602.
(80) Efremov, R. G., Feofanov, A. V., and Nabiev, I. R. (1992) Effect of hydrophobic environment on the resonance Raman spectra of tryptophan residues in proteins. *J. Raman Spectrosc. 23*, 69−73.
(81) Schlamadinger, D. E., Gable, J. E., and Kim, J. E. (2009) Hydrogen-bonding and solvent polarity markers in the UV resonance Raman spectrum of tryptophan: Application to membrane proteins. *J. Phys. Chem. B 113*, 14769−14778.
(82) Hildebrandt, P. G., Copeland, R. A., Spiro, T. G., Otlewski, J., Laskowski, M., and Prendergast, F. G. (1988) Tyrosine hydrogen-bonding and environmental effects in proteins probed by ultraviolet resonance Raman spectroscopy. *Biochemistry 27*, 5426−5433.
(83) Ludwig, B., and Asher, S. A. (1988) Ultraviolet resonance Raman excitation profiles of tyrosine: Dependence of Raman cross sections on excited-state intermediates. *J. Am. Chem. Soc. 110*, 1005−1011.
(84) Asher, S. A., and Murtaugh, J. L. (1988) UV Raman excitation profiles of imidazole, imidazolium, and water. *Appl. Spectrosc. 42*, 83−90.
(85) Takeuchi, H. (2003) Raman structural markers of tryptophan and histidine side chains in proteins. *Biopolymers 72*, 305−317.
(86) Schlamadinger, D. E., Leigh, B. S., and Kim, J. E. (2012) UV Resonance Raman study of TrpZip2 and related peptides: π-π interactions of tryptophan. *J. Raman Spectrosc. 43*, 1459−1464.
(87) Caswell, D. S., and Spiro, T. G. (1986) Ultraviolet resonance Raman spectroscopy of imidazole, histidine, and Cu(imidazole)v2+: Implications for protein studies. *J. Am. Chem. Soc. 108*, 6470−6477.
(88) Miura, T., Takeuchi, H., and Harada, I. (1988) Characterization of individual tryptophan side chains in proteins using Raman spectroscopy and hydrogen-deuterium exchange kinetics. *Biochemistry 27*, 88−94.
(89) Miura, T., Takeuchi, H., and Harada, I. (1989) Tryptophan Raman bands sensitive to hydrogen bonding and side-chain conformation. *J. Raman Spectrosc. 20*, 667−671.
(90) Harada, I., Miura, T., and Takeuchi, H. (1986) Origin of the doublet at 1360 and 1340 cm^{-1} in the Raman spectra of tryptophan and related compounds. *Spectrochim. Acta 42A*, 307−312.
(91) Takeuchi, H., Watanabe, N., Satoh, Y., and Harada, I. (1989) Effects of hydrogen bonding on the tyrosine Raman bands in the 1300−1150 cm-1 region. *J. Raman Spectrosc. 20*, 233−237.

DOI: 10.1021/acs.biochem.5b00514
Biochemistry 2015, 54, 4770−4783

(92) Strickland, E. H., and Beychok, S. (1974) Aromatic contributions to circular dichroism spectra of proteins. *Crit. Rev. Biochem. Mol. Biol. 2*, 113−175.
(93) Nagai, M., Nagatomo, S., Nagai, Y., Ohkubo, K., Imai, K., and Kitagawa, T. (2012) Near-UV circular dichroism and UV resonance Raman spectra of individual tryptophan residues in human hemoglobin and their changes upon the quaternary structure transition. *Biochemistry 51*, 5932−5941.
(94) Nagatomo, S., Nagai, M., Ogura, T., and Kitagawa, T. (2013) Near-UV circular dichroism and UV resonance Raman spectra of tryptophan residues as a structural marker of proteins. *J. Phys. Chem. B 117*, 9343−9353.
(95) (2008) The Universal Protein Resource (UniProt). *Nucleic Acids Res. 36*, D190−D195 DOI: 10.1093/nar/gkm895.
(96) White, S. H., Ladokhin, A. S., Jayasinghe, S., and Hristova, K. (2001) How membranes shape protein structure. *J. Biol. Chem. 276*, 32395−32398.
(97) Gallivan, J. P., and Dougherty, D. A. (1999) Cation-π interactions in structural biology. *Proc. Natl. Acad. Sci. U. S. A. 96*, 9459−9464.
(98) Millefiori, S., Alparone, A., Millefiori, A., and Vanella, A. (2008) Electronic and vibrational polarizabilities of the twenty naturally occurring amino acids. *Biophys. Chem. 132*, 139−147.
(99) Wimley, W. C., and White, S. H. (1996) Experimentally determined hydrophobicity scale for proteins at membrane interfaces. *Nat. Struct. Biol. 3*, 842−848.
(100) Killian, J. A., and von Heijne, G. (2000) How proteins adapt to a membrane-water interface. *Trends Biochem. Sci. 25*, 429−434.
(101) White, S. H., and Wimley, W. C. (1999) Membrane protein folding and stability: Physical principles. *Annu. Rev. Biophys. Biomol. Struct. 28*, 319−365.
(102) Sanchez, K. M., Gable, J. E., Schlamadinger, D. E., and Kim, J. E. (2008) Effects of tryptophan microenvironment, soluble domain, and vesicle size on the thermodynamics of membrane protein folding: Lessons from the transmembrane protein OmpA. *Biochemistry 47*, 12844−12852.
(103) Hong, H., Park, S., Flores Jimenez, R. H., Rinehart, D., and Tamm, L. K. (2007) Role of aromatic side chains in the folding and thermodynamic stability of integral membrane proteins. *J. Am. Chem. Soc. 129*, 8320−8327.
(104) Blondelle, S. E., and Houghten, R. A. (1991) Probing the relationships between the structure and hemolytic activity of melittin with a complete set of leucine substitution analogs. *Peptide Res. 4*, 12−18.
(105) Andreu, D., Merrifield, R. B., Steiner, H., and Boman, H. G. (1985) N-terminal analogues of cecropin A: Synthesis, antibacterial activity, and conformational properties. *Biochemistry 24*, 1683−1688.
(106) El-Mashtoly, S. F., Takahashi, H., Shimizu, T., and Kitagawa, T. (2007) Ultraviolet resonance Raman evidence for utilization of the heme 6-propionate hydrogen-bond network in signal transmission from heme to protein in *Ec* DOS protein. *J. Am. Chem. Soc. 129*, 3556−3563.
(107) Miura, T., Takeuchi, H., and Harada, I. (1991) Raman spectroscopic characterization of tryptophan side chains in lysozyme bound to inhibitors: Role of the hydrophobic box in the enzymatic function. *Biochemistry 30*, 6074−6080.
(108) Xue, Y., Davis, A. V., Balakrishnan, G., Stasser, J. P., Staehlin, B. M., Focia, P., Spiro, T. G., Penner-Hahn, J. E., and O'Halloran, T. V. (2008) Cu(I) recognition via cation-π and methionine interactions in CusF. *Nat. Chem. Biol. 4*, 107−109.
(109) Di Lella, S., Ma, L., Díaz Ricci, J. C., Rabinovich, G. A., Asher, S. A., and Álvarez, R. M. S. (2009) Critical role of the solvent environment in galectin-1 binding to the disaccharide lactose. *Biochemistry 48*, 786−791.
(110) Wen, Z. Q., and Thomas, G. J., Jr. (2000) Ultraviolet-resonance Raman spectroscopy of the filamentous virus Pf3: Interactions of Trp38 specific to the assembled virion subunit. *Biochemistry 39*, 146−152.
(111) Takeuchi, H. (2011) UV Raman markers for structural analysis of aromatic side chains in proteins. *Anal. Sci. 27*, 1077−1086.
(112) Fujimaki, N., Kitamura, F., and Takeuchi, H. (2013) Pro-oxidant copper-binding mode of the apo form of ALS-linked SOD1 mutant H43R denatured at physiological temperature. *Biochemistry 52*, 5184−5194.
(113) Hiramatsu, H., Takeuchi, K., and Takeuchi, H. (2013) Involvement of histidine residues in the pH-dependent β-galactoside binding activity of human galectin-1. *Biochemistry 52*, 2371−2380.
(114) Wang, D., Zhao, X., Vargek, M., and Spiro, T. G. (2000) Metal-bound histidine modes in UV resonance Raman spectra of Cu, Zn superoxide dismutase. *J. Am. Chem. Soc. 122*, 2193−2199.
(115) Arzhantsev, S., Vilker, V., and Kauffman, J. (2012) Deep-ultraviolet (UV) resonance Raman spectroscopy as a tool for quality control of formulated therapeutic proteins. *Appl. Spectrosc. 66*, 1262−1268.
(116) Ashton, L., Xu, Y. H., Brewster, V. L., Cowcher, D. P., Sellick, C. A., Dickson, A. J., Stephens, G. M., and Goodacre, R. (2013) The challenge of applying Raman spectroscopy to monitor recombinant antibody production. *Analyst 138*, 6977−6985.
(117) Couling, V. W., Fischer, P., Klenerman, D., and Huber, W. (1998) Ultraviolet resonance Raman study of drug binding in dihydrofolate reducase, gyrase, and catechol o-methyltransferase. *Biophys. J. 75*, 1097−1106.
(118) Hashimoto, S., Yabusaki, T., Takeuchi, H., and Harada, I. (1995) Structure and ligand-binding modes of human serum albumin studied by UV resonance Raman spectroscopy. *Biospectroscopy 1*, 375−385.
(119) Huang, C.-Y., Balakrishnan, G., and Spiro, T. G. (2005) Early events in apomyoglobin unfolding probed by laser T-jump/UV resonance Raman spectroscopy. *Biochemistry 44*, 15734−15742.
(120) Balakrishnan, G., Case, M. A., Pevsner, A., Zhao, X. J., Tengroth, C., McLendon, G. L., and Spiro, T. G. (2004) Time-resolved absorption and UV resonance Raman spectra reveal stepwise formation of T quaternary contacts in the allosteric pathway of hemoglobin. *J. Mol. Biol. 340*, 843−856.
(121) Mizuno, M., Hamada, N., Tokunaga, F., and Mizutani, Y. (2007) Picosecond protein response to the chromophore isomerization of photoactive yellow protein: Selective observation of tyrosine and tryptophan residues by time-resolved ultraviolet resonance Raman spectroscopy. *J. Phys. Chem. B 111*, 6293−6296.
(122) Sato, A., Gao, Y., Kitagawa, T., and Mizutani, Y. (2007) Primary protein response after ligand photodissociation in carbonmonoxy myoglobin. *Proc. Natl. Acad. Sci. U. S. A. 104*, 9627−9632.
(123) Rodriguez-Mendieta, I. R., Spence, G. R., Gell, C., Radford, S. E., and Smith, D. A. (2005) Ultraviolet resonance Raman studies reveal the environment of tryptophan and tyrosine residues in the native and partially unfolded states of the E colicin-binding immunity protein Im7. *Biochemistry 44*, 3306−3315.
(124) Chi, Z., and Asher, S. A. (1999) Ultraviolet resonance Raman examination of horse apomyoglobin acid unfolding intermediates. *Biochemistry 38*, 8196−8203.
(125) Weeks, C. L., Polishchuk, A., Getahun, Z., DeGrado, W. F., and Spiro, T. G. (2008) Investigation of an unnatural amino acid for use as a resonance Raman probe: Detection limits and solvent and temperature dependence of the νC$\equiv$N band of 4-cyanophenylalanine. *J. Raman Spectrosc. 39*, 1606−1613.
(126) Copeland, R. A., and Spiro, T. G. (1986) Ultraviolet resonance Raman spectroscopy of flavin mononucleotide and flavin adenine dinucleotide. *J. Phys. Chem. 90*, 6648−6654.
(127) Ames, J. B., Bolton, S. R., Netto, M. M., and Mathies, R. A. (1990) Ultraviolet resonance Raman spectroscopy of bacteriorhodopsin: Evidence against tyrosinate in the photocycle. *J. Am. Chem. Soc. 112*, 9007−9009.
(128) Harada, I., Yamagishi, K., Uchida, K., and Takeuchi, H. (1990) Ultraviolet resonance Raman spectra of bacteriorhodopsin in the light-adapted and dark-adapted states. *J. Am. Chem. Soc. 112*, 2443−2445.
(129) Ames, J. B., Ros, M., Raap, J., Lugtenburg, J., and Mathies, R. A. (1992) Time-resolved ultraviolet resonance Raman studies of protein

DOI: 10.1021/acs.biochem.5b00514
Biochemistry 2015, 54, 4770−4783

structure: Application to bacteriorhodopsin. *Biochemistry 31*, 5328−5334.
(130) Hashimoto, S., Sasaki, M., Takeuchi, H., Needleman, R., and Lanyi, J. K. (2002) Changes in hydrogen bonding and environment of tryptophan residues on helix F in bacteriorhodopsin during the photocycle: a time-resolved ultraviolet resonance Raman study. *Biochemistry 41*, 6495−6503.
(131) Asakawa, K., Masuda, S., and Takeuchi, H. (2006) Indole ring orientations of Trp189 in the ground and M intermediate of bacteriorhodopsin as studied by polarized UV resonance Raman spectroscopy. *J. Raman Spectrosc. 37*, 255−262.
(132) Hashimoto, S., Obata, K., Takeuchi, H., Needleman, R., and Lanyi, J. K. (1997) Ultraviolet resonance Raman spectra of Trp-182 and Trp-189 in bacteriorhodopsin: novel information on the structure of Trp-182 and its steric interaction with retinal. *Biochemistry 36*, 11583−11590.
(133) Kaminaka, S., and Mathies, R. A. (1999) Time-resolved ultraviolet resonance Raman of protein structural changes in the KL-intermediate of bacteriorhodopsin. *Laser Chem. 19*, 165−168.
(134) Mizuno, M., Shibata, M., Yamada, J., Kandori, H., and Mizutani, Y. (2009) Picosecond time-resolved ultraviolet resonance Raman spectroscopy of bacteriorhodopsin: Primary protein response to the photoisomerization of retinal. *J. Phys. Chem. B 113*, 12121−12128.
(135) Hashimoto, S., Sasaki, M., and Takeuchi, H. (1998) Ultraviolet resonance Raman evidence for the opening of a water-permeable channel in the M to N transition of bacteriorhodopsin. *J. Am. Chem. Soc. 120*, 443−444.
(136) Kochendoerfer, G. G., Kaminaka, S., and Mathies, R. A. (1997) Ultraviolet resonance Raman examination of the light-induced protein structural changes in rhodopsin activation. *Biochemistry 36*, 13153−13159.
(137) Hashimoto, S., Takeuchi, H., Nakagawa, M., and Tsuda, M. (1996) Ultraviolet resonance Raman evidence for the absence of tyrosinate in octopus rhodopsin and the participation of Trp residues in the transition to acid metarhodopsin. *FEBS Lett. 398*, 239−242.
(138) Chen, J., and Barry, B. A. (2008) Ultraviolet resonance Raman microprobe spectroscopy of photosystem II. *Photochem. Photobiol. 84*, 815−818.
(139) Aki, M., Ogura, T., Shinzawa-Itoh, K., Yoshikawa, S., and Kitagawa, T. (2000) A new measurement system for UV resonance Raman spectra of large proteins and its application to cytochrome *c* oxidase. *J. Phys. Chem. B 104*, 10765−10774.
(140) Halsey, C. M., Oshokoya, O. O., Jiji, R. D., and Cooley, J. W. (2011) Deep-UV resonance Raman analysis of the *Rhodobacter capsulatus* cytochrome bc_1 complex reveals a potential marker for the transmembrane peptide backbone. *Biochemistry 50*, 6531−6538.
(141) Sanchez, K. M., Kang, G., Wu, B., and Kim, J. E. (2011) Tryptophan-lipid interactions in membrane protein folding probed by UV resonance Raman and fluorescence spectroscopy. *Biophys. J. 100*, 2121−2130.
(142) Sanchez, K. M., Neary, T. J., and Kim, J. E. (2008) UV resonance Raman spectroscopy of folded and unfolded states of an integral membrane protein. *J. Phys. Chem. B 112*, 9507−9511.
(143) Oladepo, S. A., Xiong, K., Hong, Z., and Asher, S. A. (2011) Elucidating peptide and protein structure and dynamics: UV resonance Raman spectroscopy. *J. Phys. Chem. Lett. 2*, 334−344.
(144) Shafaat, H. S., Sanchez, K. M., Neary, T. J., and Kim, J. E. (2009) Ultraviolet resonance Raman spectroscopy of a β-sheet peptide: A model for membrane protein folding. *J. Raman Spectrosc. 40*, 1060−1064.
(145) Wimley, W. C., Hristova, K., Ladokhin, A. S., Silvestro, L., Axelsen, P. H., and White, S. H. (1998) Folding of β-sheet membrane proteins: A hydrophobic hexapeptide model. *J. Mol. Biol. 277*, 1091−1110.
(146) Halsey, C. M., Xiong, J., Oshokoya, O. O., Johnson, J. A., Shinde, S., Beatty, J. T., Ghirlanda, G., JiJi, R. D., and Cooley, J. W. (2011) Simultaneous observation of peptide backbone lipid solvation and α-helical ptructure by deep-UV resonance Raman spectroscopy. *ChemBioChem 12*, 2125−2128.
(147) Brown, M. C., Yakubu, R. A., Taylor, J., Halsey, C. M., Xiong, J., Jiji, R. D., and Cooley, J. W. (2014) Bilayer surface association of the pHLIP peptide promotes extensive backbone desolvation and helically-constrained structures. *Biophys. Chem. 187*−*188*, 1−6.
(148) Brogden, K. A. (2005) Antimicrobial peptides: Pore formers or metabolic inhibitors in bacteria? *Nat. Rev. Microbiol. 3*, 238−250.
(149) Zasloff, M. (2002) Antimicrobial peptides of multicellular organisms. *Nature 415*, 389−395.
(150) Epand, R. M., and Vogel, H. J. (1999) Diversity of antimicrobial peptides and their mechanism of action. *Biochim. Biophys. Acta, Biomembr. 1462*, 11−28.
(151) Blondelle, S. E., and Houghten, R. A. (1991) Hemolytic and antimicrobial activities of the twenty-four individual omission analogs of melittin. *Biochemistry 30*, 4671−4678.
(152) Wei, G., Pazgier, M., De Leeuw, E., Rajabi, M., Li, J., Zou, G., Jung, G., Yuan, W., Lu, W.-Y., Lehrer, R. I., and Lu, W. (2010) Trp-26 imparts functional versatility to human α-defensin HNP1. *J. Biol. Chem. 285*, 16275−16285.
(153) Andreu, D., Merrifield, R. B., Steiner, H., and Boman, H. G. (1985) N-terminal analogues of cecropin A: Synthesis, antibacterial activity, and conformational properties. *Biochemistry 24*, 1683−1688.
(154) Gable, J. E., Schlamadinger, D. E., Cogen, A. L., Gallo, R. L., and Kim, J. E. (2009) Fluorescence and UV resonance Raman study of peptide-vesicle interactions of human cathelicidin LL-37 and its F6W and F17W mutants. *Biochemistry 48*, 11264−11272.
(155) Turner, J., Cho, Y., Dinh, N.-N., Waring, A. J., and Lehrer, R. I. (1998) Activities of LL-37, a cathelin-associated antimicrobial peptide of human neutrophils. *Antimicrob. Agents Chemother. 42*, 2206−2214.
(156) Dürr, U. H. N., Sudheendra, U. S., and Ramamoorthy, A. (2006) LL-37, the only human member of the cathelicidin family of antimicrobial peptides. *Biochim. Biophys. Acta, Biomembr. 1758*, 1408−1425.
(157) Quan, B., and Ianoul, A. (2009) UV resonance Raman spectroscopy probes the localization of tryptophan-containing antimicrobial peptides in lipid vesicles. *J. Raman Spectrosc. 40*, 260−263.
(158) Strøm, M. B., Rekdal, Ø., and Svendsen, J. S. (2000) Antibacterial activity of 15-residue lactoferricin derivatives. *J. Pept. Res. 56*, 265−274.
(159) Santamaría, C., Larios, S., Quirós, S., Pizarro-Cerda, J., Gorvel, J. P., Lomonte, B., and Moreno, E. (2005) Bactericidal and antiendotoxic properties of short cationic peptides derived from a snake venom lys49 phospholipase A_2. *Antimicrob. Agents Chemother. 49*, 1340−1345.
(160) Pripotnev, S., Won, A., and Ianoul, A. (2010) The effects of L- to D-isomerization and C-terminus deamidation on the secondary structure of anitmicrobial peptide Anoplin in aqueous and membrane mimicking environment. *J. Raman Spectrosc. 41*, 1645−1649.
(161) Schlamadinger, D. E., Wang, Y., McCammon, J. A., and Kim, J. E. (2012) Spectroscopic and computational study of melittin, cecropin A, and the hybrid peptide CM15. *J. Phys. Chem. B 116*, 10600−10608.
(162) Lührs, T., Ritter, C., Adrian, M., Riek-Loher, D., Bohrmann, B., Döbeli, H., Schubert, D., and Riek, R. (2005) 3D structure of Alzheimer's amyloid-β(1−42) fibrils. *Proc. Natl. Acad. Sci. U. S. A. 102*, 17342−17347.
(163) Sikirzhytski, V., Topilina, N. I., Higashiya, S., Welch, J. T., and Lednev, I. K. (2008) Genetic engineering combined with deep UV resonance Raman spectroscopy for structural characterization of amyloid-like fibrils. *J. Am. Chem. Soc. 130*, 5852−5853.
(164) Pawar, A. P., DuBay, K. F., Zurdo, J., Chiti, F., Vendruscolo, M., and Dobson, C. M. (2005) Prediction of "aggregation-prone" and "aggregation-susceptible" regions in proteins associated with neurodegenerative diseases. *J. Mol. Biol. 350*, 379−392.
(165) Popova, L. A., Kodali, R., Wetzel, R., and Lednev, I. K. (2010) Structural variations in the cross-β core of amyloid β fibrils revealed by deep UV resonance Raman spectroscopy. *J. Am. Chem. Soc. 132*, 6324−6328.

DOI: 10.1021/acs.biochem.5b00514
Biochemistry 2015, 54, 4770−4783

(166) Wang, M., and JiJi, R. D. (2011) Resolution of localized small molecule-Aβ interactions by deep-ultraviolet resonance Raman spectroscopy. *Biophys. Chem. 158*, 96−103.
(167) Cheng, H., Xia, B., Reed, G. H., and Markley, J. L. (1994) Optical, EPR, and H-1 NMR spectroscopy of serine-ligated [2Fe-2S] ferredoxins produced by site-directed mutagenesis of cysteine residues in recombinant *anabaena* 7120 vegetative ferredoxin. *Biochemistry 33*, 3155−3164.
(168) Oelze, J. (1985) Analysis of Bacteriochlorophylls. *Methods Microbiol. 18*, 257−284.
(169) Kobayashi, M., Akiyama, M., Kano, H., and Kise, H. (2006) Spectroscopy and structure determination. In *Chlorophylls and Bacteriochlorophylls: Biochemistry, Biophysics, Functions and Applications* (Grimm, B., Porra, R. J., Rudiger, W., and Scheer, H., Eds.) Springer, Dordrecht, The Netherlands.

DOI: 10.1021/acs.biochem.5b00514
Biochemistry 2015, 54, 4770−4783